Molecular Mechanisms that Regulate the Coupled Period of the Mammalian Circadian Clock

Jae Kyoung Kim,[†*] Zachary P. Kilpatrick,[‡] Matthew R. Bennett,[§¶] and Krešimir Josić[‡||*]

[†]Mathematical Biosciences Institute, The Ohio State University, Columbus, Ohio; [‡]Department of Mathematics, University of Houston, Houston, Texas; [§]Department of Biochemistry & Cell Biology and [¶]Institute of Biosciences and Bioengineering, Rice University, Houston, Texas; and [||]Department of Biology and Biochemistry,Te5of Houstonartm.6(e7401e7,86-1.1s;)-289.631279cwf16638.192Tm()T70ST1(12RC4ns192T12(12RC4

and population mean, inconsistent with experimental findings (Fig. 1) (13–15).

Previous mathematical models have typically relied on Hill functions to describe transcriptional repression in the negative feedback loop (13–15). However, in a recent theoretical study it was shown that circadian clocks behave very differently when transcriptional repression occurs via protein sequestration, in which repressor inhibits a transcriptional activator via 1:1 stoichiometric binding (Fig. 2 *A*), rather than highly nonlinear Hill-type regulation (Fig. 2 *B* and see Fig. S1 in the Supporting Material) (23). That is, a model based on protein sequestration successfully reproduced various experimental observations that have not been addressed by previous models based on Hill-type regulation, such as the importance of a 1:1 molar ratio between repressor and activator and an additional negative feedback loop via Rev-erbα/β for robust circadian timekeeping (23–25). This indicates that the mechanism of transcriptional regulation plays a key role in determining the behaviors of circadian clocks.

Interestingly, recent experimental studies have found that protein sequestration is responsible for repression in the negative feedback loops of circadian clocks in multicellular organisms (*D* ; € and mammals), which have intercellular coupling among the pacemaker cells in the brain (24,26,27,29). In contrast, a phosphorylation-based repression mechanism appears to be used in organisms which do not have this intercellular coupling. In a syncytium, , the repressors transiently bind activators and induce phosphorylation at multiple activator sites, and thus repress its transcriptional activity (see Fig. S1) (30). A similar phosphorylation-based repression mechanism is used in a unicellular organism, cyanobacteria, in which KaiA phosphorylates the multiple sites of KaiC (31), which leads to Hill-type regulation (32,33). These different repression mechanisms of organisms depending on the presence of intercellular coupling raises the question of whether the transition to protein sequestration is important for synchronizing the rhythms of multiple cells.

Here, we show that when transcriptional repression occurs via protein sequestration, but not Hill-type regulation, the coupled periods are near the mean period of the individual cells within the SCN. To do this, we first compare

loop (~24 h) to synchronize rhythms with the period close to the population mean.

We found that the mechanisms underlying the intracellular feedback loop play a pivotal role in regulating the coupled period. This reveals that two of the major functions of the SCN—the generation of a rhythm within a cell and synchronization of the rhythm across the population—are closely related. Furthermore, these findings indicate that the intracellular feedback mechanism of multicellular organisms—a different type of mechanism from

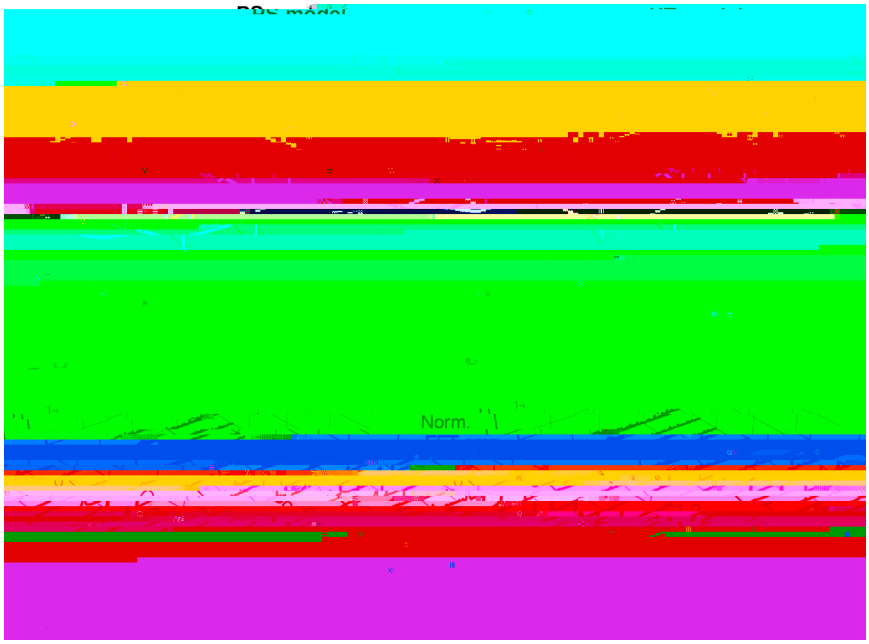

FIGURE 4 The coupled periods of heterogeneous cells in the PS and HT model. (*A*) When a fast cell and a slow cell are coupled, the coupled frequencies, at which two cells synchronize, of the PS model are similar to the mean frequency of uncoupled cells, but (*B*) those of HT model is greater than the mean frequency. Frequencies are estimated using a fast Fourier transform and normalized to make the mean frequency unity. Two different frequencies of single cell models are obtained by dividing all production and degradation rates by common rescaling factors of 1 and 1.2, respectively. These results are robust against parameter changes (see Fig. S3) and the introduction of nonlinearities in the coupling (see Fig. S4). Here, we represent the results involving = 0, 0.05, 0.1, …, 0.3. (*C*) When 100 cells with different periods are coupled, the coupled frequencies of the PS model converge to the mean frequency of uncoupled cells, but (*D*) those of the HT model become larger than the mean frequency. Here, 100 rescaling factors for different frequencies are drawn randomly from a normal distribution of mean 1 and standard deviation 0.15, matching the experimental data (Fig. 1, *A* and *B*). See Fig. S6 for stronger coupling strengths and Fig. S7 for cell populations with larger heterogeneities. To see this figure in color, go online.

intermediate reaction steps, which allows the model to oscillate with a lower Hill coefficient (32,39,40). Even with a low Hill coefficient, the coupled period of the model is still far from the mean period in this extended HT model (see Fig. S5).

The coupled periods of heterogeneous cell population

Next, we test how the coupling affects the periods in a population of 100 cells with different intrinsic periods. To achieve heterogeneity we again rescale the time of each cell in the population using 100 rescaling factors sampled from a normal distribution with mean 1 and standard deviation 0.15. This generates variability in periods similar to that observed in the SCN (Fig. 1) (7,8,50). In the PS model, increasing coupling strength again causes the frequencies of individual cells to cluster around the population mean of the uncoupled cells (Fig. 4 *C*). When coupling strength exceeds a threshold (~ 0.3), rhythms are synchronized with frequencies close to the population mean (Fig. 4 *C*). However, in the HT model, as coupling strength increases, frequencies cluster around a value greater than the mean frequency of the uncoupled cells (Fig. 4 *D*). When the coupling strength exceeds a threshold (~ 0.3), the population synchronizes at a frequency significantly above the population mean (Fig. 4 *D*). The frequencies of the coupled HT model only approach the population mean when the coupling strength far exceeds the threshold (~ 1) (see Fig. S6). With coupling this strong, the coupled frequencies of the PS model become slightly smaller than the mean frequency (see Fig. S6). However, experimental evidence suggests that the coupling strength is much smaller than unity (47). Furthermore, the HT model can exhibit synchronous oscillations at a frequency close to the population mean only at an unrealistically large coupling strength. This would require a large amount of neurotransmitters at a high cost to the organism. Thus, the PS model with the weak coupling provides a more efficient mechanism for synchrony than the HT model with strong coupling. We also examine systems of oscillators whose distribution of uncoupled periods had a larger variability. Even in this case, the PS model synchronizes at frequencies that are close to the population mean (see Fig. S7 *A*). However, the frequencies of the synchronized HT model are again much larger than the mean with the realistic coupling strength (see Fig. S7 *B*).

iPRCs and average interaction functions (AIFs) of PS model and HT model

We have shown that the period of the synchronous population is close to the population mean for the PS model, but significantly shorter than the population mean for the HT model (Fig. 4). To understand the mechanisms that underlie this difference, we employ the theory for weakly coupled oscillators, which has been used widely to understand synchronization in networks of oscillators (51–53). Assuming weak coupling (47), the theory allows us to describe the essential dynamics of the four-dimensional cell model (Eq. 5) using a single differential equation for the phase of the limit cycle.

To derive the equation for the phase dynamics, first, we need to estimate the iPRCs, ( ), in response to mRNA perturbation,

$$Z(\ ) = \lim_{\Delta M \to 0} \frac{\Delta}{\Delta M},$$

where Δ represents the brief perturbation of mRNA and Δ represents the phase change due to the perturbation of mRNA. Numerically we calculate the iPRCs for both the PS and HT models (54). The advance and delay region of the iPRC are balanced in the PS model (Fig. 5 *A*), whereas the advance regions of the iPRC is much larger than the delay region in the HT model (Fig. 5 *B*). Importantly, the iPRC of the PS model more closely resembles the experimentally measured PRC than does the iPRC of the HT model. When the PRC is measured in response to 100 nM VIP in the SCN, the delay region is slightly larger than the advance region (47).

Next, we explore why the iPRC of the PS model is more balanced than that of the HT model. To do this, we analyze the magnitudes of the maxima and minima of the iPRCs in the models, which indicate the largest phase advance and delay, respectively. We found that the extrema of the iPRC occur when the time derivative of the mRNA is zero—i.e., when the transcription and degradation rates of the mRNA are equal (arrows in Fig. 5, *C* and *D*). This occurs because the phase of the oscillation is most sensitive to mRNA changes when the time derivative of the mRNA is zero (see the Appendix). Furthermore, we found that the slope of the transcription rate at these times appears to determine the extrema of the iPRC. That is, the maximum and minimum of the iPRC is approximately proportional to the inverse of the slope of transcription rates (see Appendix for details)

$$Z(\ )_{\text{extrema}} \approx \frac{}{\beta} \frac{-W\ \ - e^{-e^{-T}-T}}{+W(-e^{-e^{-T}-T})} \propto \frac{}{\beta},$$

where β is the slope of transcription rates at the phase when the iPRC is extrema, is the reference time, and is the Lambert function—a branch of the inverse of . When the iPRC attains its maximum or minimum, the steepness of transcription rates is similar in the PS modelverse of

$$\frac{d}{dt} = w' -$$

than sigmoidal (Fig. 2 *D*), the iPRCs and AIFs are balanced (Fig. 5 *E*), and the coupled periods are close to the population mean period (Fig. 4 *B* and *D*). Interestingly, only protein sequestration appears to lead piecewise linear gene regulation among other proposed rhythm generating mechanisms such as oligomerization, multiple phosphorylation, and cooperative enzyme kinetics (32). However, it would be interesting to examine further if such exist and study their effect on synchronous oscillations.

Circadian clocks are widely found in organisms as diverse as bacteria, algae, plants, fungi, insects, and mammals (56). Whereas each of these organisms appear to use an intracellular negative feedback loop to generate circadian rhythms, there is a variety of mechanisms by which negative feedback is mediated. In mammals and *D* , the repressor (PER) appears to inhibit the activator (BMAL1-CLOCK in mammals and CYC-CLK in *D*) through protein sequestration. In both of these clocks, repressors tightly bind activators in a 1:1 stoichiometric complex, prohibiting activators from binding DNA (24,26,27,29). In contrast, a phosphorylation-based repression mechanism appears to be used in (see Fig. S1). Here, the repressor (FRQ) binds the activator (WC complex) transiently and recruits kinases, which phosphorylate multiple sites of the activator (WC complex) and represses the transcriptional activity of the activator (30). Furthermore, the repressor concentration in is much lower than that of the activator in nucleus, because kinase at low concentration is usually enough to phosphorylate its substrate (57–59). A similar phosphorylation-based repression mechanism is used in cyanobacteria, in which KaiA phosphorylates the multiple-sites of KaiC (31).

Taken together, protein sequestration appears to be used as a repression mechanism in multicellular organisms, mammals, and *D* , but not in a syncytium, - and a unicellular organism, cyanobacteria. This raises the question of why different mechanisms are used for transcriptional regulation depending on the type of organism. It

region of SCN (5,6). Future models should include various neurotransmitters and spatial heterogeneity with various network architecture of coupling (15). Testing our predic-

Foundation grant No. DMS-0931642 to the Mathematical Biosciences Institute (to J.K.K.).

REFERENCES

1. Dibner, C., U. Schibler, and U. Albrecht. 2010. The mammalian circadian timing system: organization and coordination of central and peripheral clocks. *A€*. . . . 72:517–549.
2. Antle, M. C., and R. Silver. 2005. Orchestrating time: arrangements of the brain circadian clock. . 28:145–151.
3. K729-0iol.